Accepted Manuscript

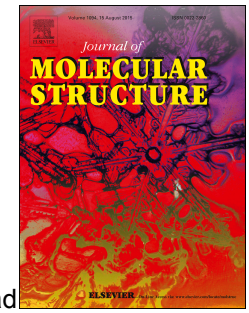

New spiro-oxindole constructed with pyrrolidine/thioxothiazolidin-4-one derivatives: Regioselective synthesis, X-ray crystal structures, Hirshfeld surface analysis, DFT, docking and antimicrobial studies

Assem Barakat, Saied M. Soliman, Abdullah Mohammed Al-Majid, M. Ali, Mohammad Shahidul Islam, Yaseen A.M.M. Elshaier, Hazem A. Ghabbour

PII: S0022-2860(17)31284-X

DOI: 10.1016/j.molstruc.2017.09.086

Reference: MOLSTR 24335

To appear in: *Journal of Molecular Structure*

Received Date: 14 June 2017

Revised Date: 21 August 2017

Accepted Date: 22 September 2017

Please cite this article as: A. Barakat, S.M. Soliman, A.M. Al-Majid, M. Ali, M.S. Islam, Y.A.M.M. Elshaier, H.A. Ghabbour, New spiro-oxindole constructed with pyrrolidine/thioxothiazolidin-4-one derivatives: Regioselective synthesis, X-ray crystal structures, Hirshfeld surface analysis, DFT, docking and antimicrobial studies, *Journal of Molecular Structure* (2017), doi: 10.1016/j.molstruc.2017.09.086.

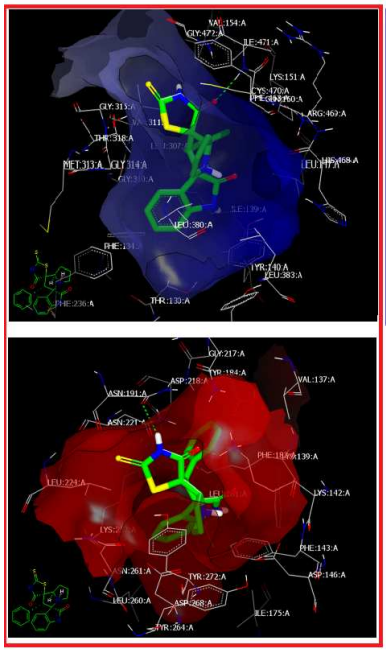

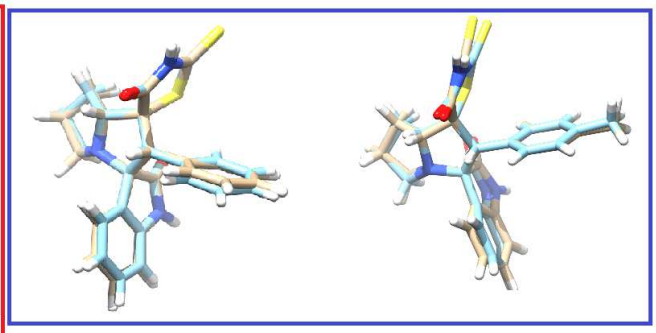

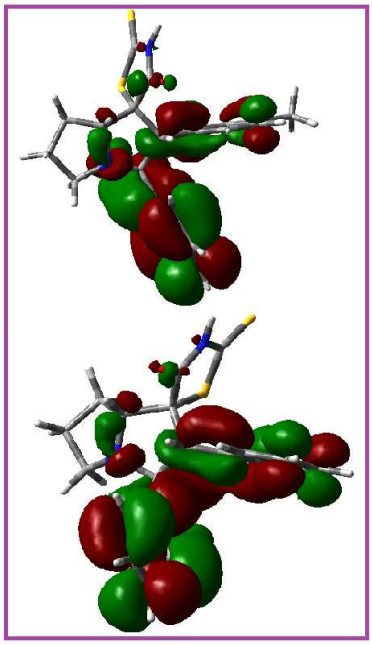

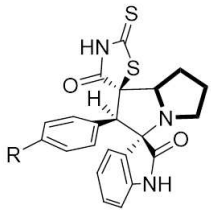

4a R = CH_3
4b R = H

@ Regioselective synthesis
@X-ray single crystal
@Hirshfeld surface analysis
@ DFT- HOMO- LUMO
@ Anti-microbial
@ Docking studies

New spiro-oxindole constructed with pyrrolidine/thioxothiazolidin-4-one derivatives: Regioselective synthesis, X-ray crystal structures, Hirshfeld surface analysis, DFT, docking and antimicrobial studies

Assem Barakat[a,c,*], Saied M. Soliman[b,c], Abdullah Mohammed Al-Majid[a], M. Ali[a], Mohammad Shahidul Islam[a], Yaseen A. M. M. Elshaier[d], and Hazem A. Ghabbour[e,f]

[a] *Department of Chemistry, College of Science, King Saud University, P.O. Box 2455, Riyadh 11451, Saudi Arabia.*

[b] *Department of Chemistry, College of Science & Arts, King Abdulaziz University, P.O. Box 344 Rabigh 21911, Saudi Arabia.*

[3c] *Department of Chemistry, Faculty of Science, Alexandria University, P.O. Box 426, Ibrahimia, Alexandria 21321, Egypt.*

[d] *Pharmaceutical Organic Chemistry Department, Faculty of Pharmacy, Al-Azhar University, Assuit 71524, Egypt.*

[e] *Department of Pharmaceutical Chemistry, College of Pharmacy, King Saud University, P. O. Box 2457, Riyadh 11451, Saudi Arabia.*

[f] *Department of Medicinal Chemistry, Faculty of Pharmacy, University of Mansoura, Mansoura 35516, Egypt.*

***** Correspondence: ambarakat@ksu.edu.sa; Tel.: +966-114-675-901; Fax: +966-114-675-992.

Abstract: In this work, polycyclic heterocycles containing spirooxindole, pyrrolidine, and thioxothiazolidin-4-one rings have been synthesized via the regioselective 1,3-dipolar cycloaddition of azomethine ylide, which is generated in situ by the condensation of the dicarbonyl compound isatin and the secondary amino acid (L-proline), with 5-arylidine-2-thioxothiazolidin-4-one as the dipolarophile. The structure of the synthesized compounds **4a** and **4b**, was determined by using X-ray single crystal diffraction, and also, Hirshfeld surface analysis were reported. Their geometric parameters were calculated using density functional theory at the B3LYP/6-311G (d,p) level of theory. Both compounds showed antimicrobial and antifungal activity better than selected standards (ampicillin and gentamicin in case of antibacterial activity and Amphotricin A and fluconazole in case of antifungal activity). Molecular docking study of the synthesized compounds indicated that phenyl group plays an important role in determination of compound interaction inside the receptors.

Keywords: spirooxindole; thioxothiazolidin-4-one; Hirshfeld surface analysis; DFT; anti-microbial activity

1. Introduction

The spirocyclic ring structure is a unique feature of a number of natural and synthetic products that possess interesting biological activities. The potential use of spiro derivatives in medicinal chemistry has been well recognized owing to their antimycobacterial, antitumor, antiproliferative, and anti-tuberculosis activities [1−15]. Similarly, the 4-thiazolidinone moiety has been utilized for the synthesis of a variety of useful heterocyclic products including drugs [16,17], dyes, and intermediates such as thioflavin T., thiazole yellow, and thidiazuron [18]. Furthermore, 4-thiazolidinone derivatives have been used as

insecticides [19,20] and herbicides [21] owing to their low toxicity toward human beings and excellent biological activity. The thiazolidinone moiety is also associated with a broad spectrum of biological activities including antidiabetic [22], antifungal, antibacterial, anti-inflammatory, anticonvulsant, hypnotic, anti-tuberculosis, antihistaminic, antiviral, cardiovascular, anthelmintic, and anticancer properties [23,24]. A number of 4-thiazolidinone derivatives have been investigated for their inhibitory effect on the oxidation of *β*-hydroxybutyrate substrate by rat brain homogenates and in the tricarboxylic acid cycle during respiratory activity [25]. Therefore, development of new spiro-heterocycles having oxindole, pyrrolidine, or thiazolidinone rings is worthwhile from the perspective of medicinal chemistry.

Recently, several methods have been reported in literature for the synthesis of oxindole derivatives with spiro heterocycles [26,27]. Generally, isatin and its derivatives have been employed as the starting materials for 1,3-dipolar cycloaddition reactions that yield the spirooxindole core owing to the facile preparation of the corresponding azomethine ylides in the presence of α-amino acids [28−33]. Ponnala et al. have reported an example of 1,3-dipolar cycloaddition reactions with olefins that proceed regio- and stereoselectively to furnish the novel dispiropyrrolidine scaffold [34]. Liu et al. have developed an efficient three-component reaction of 5-arylidene-4-thioxo-1,3-thiazolidine-2-one or 5-arylidene-1,3-thiazolidine-2,4-dione, sarcosine, and isatin for the synthesis of dispiropyrrolidine derivatives in ethanol under ultrasound irradiation [35]. Another example reported by Prasad and coworkers is a facile method for the syntheses of pyrrolizidine-substituted benzo[*h*]quinoline, quinoline, dispiropyrrolidine, and

thiapyrrolizidine compounds in good yields via multicomponent 1,3-dipolar cycloaddition reactions of azomethine ylide [36]. However, to the best of our knowledge, there are no reports on the synthesis of this regioisomers and diastereoisomers of dispiro compounds containing rhodanine.

In this work, the synthesis and X-ray crystal structures of diastereomerically pure spiro-oxindole, pyrrolidine, and thiazolidinone rings have been reported for the first time. Moreover, the anti-microbial activities and molecular docking study as well was addressed on this work.

2. Materials and Methods

2.1. General remarks

"All chemicals were purchased from Aldrich, Sigma-Aldrich, and Fluka and used without further purification, unless otherwise stated. All melting points were measured on a Gallenkamp melting point apparatus in open glass capillaries and are uncorrected. IR spectra were measured as KBr pellets on a Nicolet 6700 FT-IR spectrophotometer. NMR spectra were recorded on a Varian Mercury Jeol-400 NMR spectrometer. ^{1}H (400 MHz) and ^{13}C-NMR (100 MHz) were measured in deuterated dimethyl sulfoxide (DMSO-d_6). Chemical shifts (δ) are in ppm, and *J*-coupling constants are given in Hz. Mass spectra were recorded on a Jeol JMS-600 H instrument. Elemental analysis was carried out on an Elmer 2400 Elemental Analyzer in CHN mode. For X-ray diffraction analysis, data were collected on a Bruker APEX-II D8 Venture diffractometer with an area detector".

*3.2. General procedure for the synthesis of **4a,b** (GP1)*

A stirred mixture of isatin **2** (74 mg, 0.5 mmol), L-proline **3** (57.5 mg, 0.5 mmol), and 5-benzylidene-2-thioxothiazolidin-4-one **1a,b** (0.5 mmol) in MeOH (10 ml) was heated under reflux conditions for the specified period of time. After completion of the reaction was indicated by TLC, the solvent was evaporated under reduced pressure and the residue was purified by column chromatography using petroleum ether–ethyl acetate (3:1) as the eluent.

*(1'R,7a'R)-2''-Thioxo-2'-(p-tolyl)-5',6',7',7a'-tetrahydro-2'H-dispiro[indoline-3,3'-pyrrolizine-1',5''-thiazolidine]-2,4''-dione**, 4a***

IR (KBr, ν, cm^{-1}): 3246, 1722, 1618, 1595, 1515, 1471; ^{1}H NMR (400 MHz, DMSO-d_6) δ: 11.80 (bs, 1H, NH), 9.86 (bs, 1H, NH), 7.84−7.66 (m, 8H, Ar-H), 5.49−5.41 (d, *J* = 9.3 Hz, 1H) , 4.10 (m, 2H), 2.91 (t, 2H), 2.28 (m, 2H), 2.10 (s, 3H), 1.12 (m, 2H); ^{13}C NMR (100 MHz, DMSO-d_6) δ: 26.9, 30.6, 47.3, 51.5, 54.9, 63,6, 71.5, 73.7, 107.4, 111.9, 113.3, 122.2, 129.7, 131.5, 136.4, 144.2, 162.0, 170.2, 174.2, 178.1; HRMS *(m/z)* calculated for $[M+1]^+$ $C_{23}H_{21}N_3O_2S_2$ 435.11, found: 436.11. Elemental Analysis: C, 63.42; H, 4.86; N, 9.65; S, 14.72; found C, 63.45; H, 4.85; N, 9.70; S, 14.71.

*(1'R,7a'R)-2'-Phenyl-2''-thioxo-5',6',7',7a'-tetrahydro-2'H-dispiro[indoline-3,3'-pyrrolizine-1',5''-thiazolidine]-2,4''-dione, **4b***

IR (KBr, ν, cm^{-1}): 3340, 1710, 1610, 1466; ^{1}H NMR (400 MHz, DMSO-d_6) δ: 11.81 (bs, 1H, NH), 9.91 (bs, 2H, NH), 7.98−7.70 (m, 8H, Ar-H), 5.55−5.51 (d, *J* = 9.3 Hz, 1H) , 4.12 (m, 2H), 2.95 (t, 2H), 2.29 (m, 2H), 1.17 (m, 2H); ^{13}C NMR (100 MHz, DMSO-d_6) δ: 26.5, 48.0, 53.8, 56, 67.8, 72.6, 79.6, 83.4, 100.5, 108.3, 111.0, 122.4, 129.8, 131.4, 139.3, 144.0,

162.3, 170.0, 174.1, 178.0; HRMS *(m/z)* calculated for $C_{22}H_{19}N_3O_2S_2$ $[M+1]^+$: 421.09, found: 422.09; Elemental Analysis: C, 62.69; H, 4.54; N, 9.97; S, 15.21; found: C, 62.71; H, 4.55; N, 10.00; S, 15.22.

2.3 Computational details

The X-ray structures of the studied compounds were optimized by using the Gaussian 09 program [37,38]. For this task, the B3LYP method and 6-311G(d,p) basis sets were used for all atoms. Frequency calculations gave no imaginary frequencies, indicating that the optimized structure is an energy minimum as there were no negative modes.

2.4. Hirshfeld surface analysis

Hirshfeld surfaces (HSs) and 2D fingerprint plots (FPs) were generated by using the Crystal Explorer 3.1 software [39]. The crystallographic information files (CIF) obtained from the X-ray single crystal measurements were used for performing the HS analysis. The HSs and FPs were constructed based on the electron distribution calculated as the sum of spherical atom electron densities [40−47].

2.4. Agar Diffusion Well Method to Determine the Antimicrobial Activity

2.4.1. Antibacterial Activity of Compound **4a,b**

"Antibacterial activities were investigated by using agar well diffusion method, against the *Staphylococcus pneumonia* (RCMB 010010) and *Bacillus subtilis* (RCMB 010067) (as Gram-positive bacteria) and *Pseudomonas aeruginosa* (RCMB 010043) and *Escherichia coli* (RCMB 0100052) (as Gram-negative bacteria). The solution of 10 mg/mL of compound in DMSO was prepared for testing against bacteria. Centrifuged pellets of bacteria from 24 h

old culture containing approximately 10^4–10^6 CFU (colony forming unit) per mL were spread on the surface of nutrient agar (type tone 1%, yeast extract 0.5%, NaCl 0.5%, agar, and 1000 mL of distilled water, pH 7.0) which was autoclaved under 121 °C for at least 20 min. Wells were created in medium with the help of sterile metallic bores and then cooled down to 45 °C. The activity was determined by measuring the diameter of the inhibition zone (in mm). A volume of 100 µL of the tested sample (10 mg/mL) was loaded into the wells of the plates. A solution of the compound was prepared in DMSO, while DMSO was also loaded as control. The plates were kept for incubation at 37 °C for 24 h and then the plates were examined for the formation of zones of inhibition. Each inhibition zone was measured three times by caliper to get an average value. The test was performed three times for each bacterium and the average was taken. Ampicillin and Gentamicin were used as antibacterial standard drugs" [48].

2.4.2. Antifungal Activity of Compound **4a,b**

Tested sample was screened *in vitro* for its antifungal activity against various fungi, namely, *Aspergillus fumigatus* (RCMB 002568), *Syncephalastrumracemosum* (RCMB 016001) *Geotricumcandidum* (RCMB 05097) and *Candida albicans* (RCMB 05036). The antifungal activity was performed by agar well diffusion method [48].

"Fungal strains were grown in 5 mL Sabouraud dextrose broth (glucose/peptone; 40/10) for 3–4 days to obtain 10^5 CFU/mL cells. The fungal culture (0.1 mL) was spread uniformly on the Sabouraud dextrose agar plates by sterilized triangular folded glass rod. Plates were left for 5–10 min so the culture was properly adsorbed on the surface. Then small wells 4 mm × 2 mm were cut into the plates with the help of well cutter and the bottoms of the wells were sealed with 0.8% soft agar to prevent the flow of test sample at the bottom of the well. 100 µL of the tested sample (10 mg/mL) was loaded into the wells of the plates. Compound **1** dissolved in DMSO, while pure DMSO was also used as control. The plates were kept for incubation at 30 °C for 3–4 days and then examined for the formation of zones of inhibition. The

test was performed three times for each fungus and the average was taken. Amphotericin B/Fluconazole were used as standard antifungal drug" [48].

2.5. Docking studies

This was done using OpenEye molecular Modeling software. A virtual library of Spirooxoindile derivatives were energy minimized using MMFF94 force field, followed by generation of multi-conformers using OMEGA application. The whole energy minimized library will be docked along with the prepared PDB ID: 3HAM and PDB ID: 4WMZ using FRED application to generate a physical property (ΔG) reflecting the predicted energy profile of ligand-receptor complex. Vida application can be employed as a visualization tool to show the potential binding interactions of the ligands to the receptor of interest [49-51].

3. Results and discussion

3.1. Synthesis

Synthesis of compounds **4a** and **4b** has been achieved via the 1,3-dipolar cycloaddition reaction protocol [52] and illustrated in Scheme 1. In our initial endeavor, Knoevenagel adducts **1a, b** were prepared following our previously reported method [23]. Next, the three-component reaction between 5-arylidene-2-thioxothiazolidin-4-one (**1a** and **1b**), isatin (**2**), and L-proline (**3**) was carried out at 60 °C in refluxed MeOH, for 5−8 h to produce **4a** and **4b** with two spiro centers in regioselective manner with 85% and 89% yields, respectively. The structure of the cycloadduct was confirmed by spectroscopic analyses and it was found that the reaction afforded adducts **4a** and **4b** as single regioisomers. The structures of the

compounds were deduced by ^{1}H and ^{13}C NMR, and IR spectroscopies, MS, elemental analysis, and X-ray crystallography.

Scheme 1. Synthesis of **4a** and **4b**

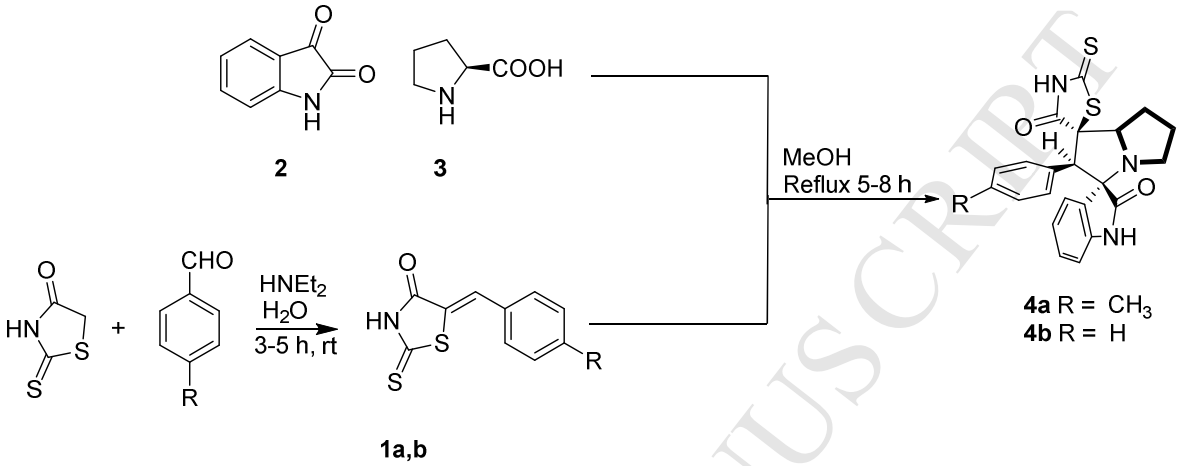

Exclusive regioselectivity of the new spiro-oxindole constructed with pyrrolidine/thioxothiazolidin-4-one derivatives formation was deduced from spectral characterization. The ^{1}H-NMR spectrum for compounds **4a** shown δ 11.81 and 9.86 (bs) for the secondary amine proton NH, at δ 7.84−7.66 (m) for the aromatic protons, at δ 5.49−5.41 (d) with J = 9.3 Hz for the benzylic proton, and the pyrrolidine ring protons have been assigned at δ 4.10, 2.91, 2.28, and 1.12 ppm and finally at δ 2.10 (s, 3H) assigned for the methyl group protons. Also, ^{13}C-NMR spectrum shown agreement with the expected compound. Moreover, the MS spectrum was also observed at 436.11*(m/z)* calculated for $[M+1]^{+}$ $C_{23}H_{21}N_3O_2S_2$. IR spectrum, which correlated with the functional groups including NH, C=C, C=S and C=O. Confirmation of the assignment of the regioisomer was achieved by X-ray single crystal diffraction technique. The crystallographic perspective drawing (Figure 1) shows that the structure of **4a** in the solid state is in full accord with the

regioisomer as elucidated in solution by spectral analysis. Similarly, the spectrum for the second new spiro-oxiindole **4b** was in full agreement with expected product.

The proposed mechanism for the synthesis of spiro-oxindolepyrrolidine thioxothiazolidin-4-one derivatives (**4**) is described in Scheme 2. The reaction proceeds via the generation of azomethine ylide (dipolar structure **6**, Scheme 2). Azomethine **6** was obtained by the condensation of isatin (2) with L-proline (3) and subsequent decarboxylation of the condensation product **5**. Dipolarophiles **1a** and **1b** react with the respective azomethine ylides (**6)** in methanol to give the desired products containing spiro-oxindole, -pyrrolidine, and -thioxothiazolidin-4-one moieties, **4a-b**. The regiochemistry of the cycloaddition reaction can be explained by considering secondary orbital interactions (SOI) of the arylidine double bond of the dipolarophile **1** with those of the ylide, as shown in Scheme 2. It is evident that the formation of regioisomer **4** via path A is more favorable, which is not possible in path B. this could be attributed due to formation of *Z* isomer of **1a-b** which allow the approach of azomethine from one side only. Hence, only one regioisomer **4** was obtained in the reaction. Furthermore, the steric factor plays an additional role in the regioselective formation of products.

Scheme 2: Plausible approaches for the target compound

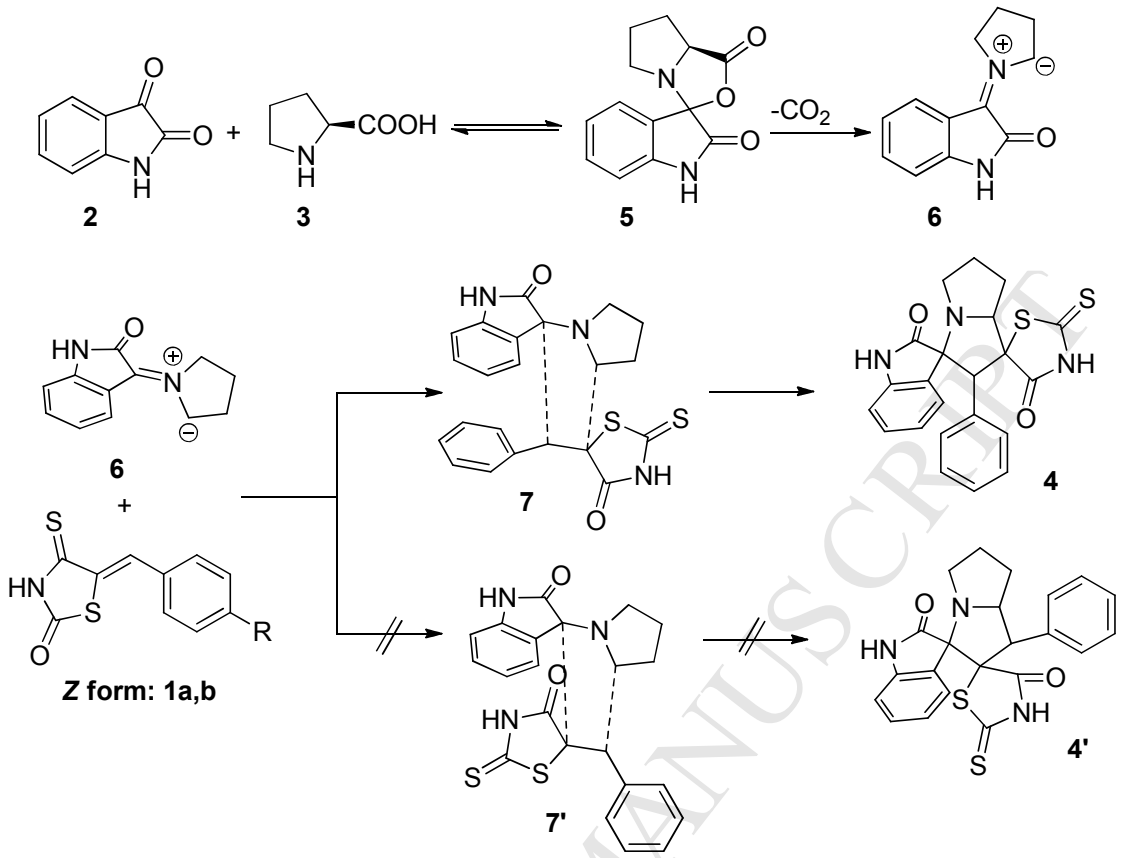

*3.2. X-ray crystal structure of compounds **4a,b***

The crystal structures of compounds **4b** and **4b** were determined by single-crystal X-ray diffraction (Figure 1) [53,54]. The crystal and structure refinement data, as well as selected geometric parameters for compounds **4b** and **4b** are given in Tables 1, 2, and 4. The asymmetric unit of **4a** and **4b** comprised one independent molecule of these compounds and the solvent molecules methanol and dichloromethane, respectively. In the crystal packing of **4a**, its molecules are linked by six hydrogen bonding interactions that result in a three-dimensional network structure (Figure 2 and Table 3). In case of **4b**, the molecules are also packed together utilizing six intermolecular interactions to form a network structure as shown in Figure 2 and Table 5.

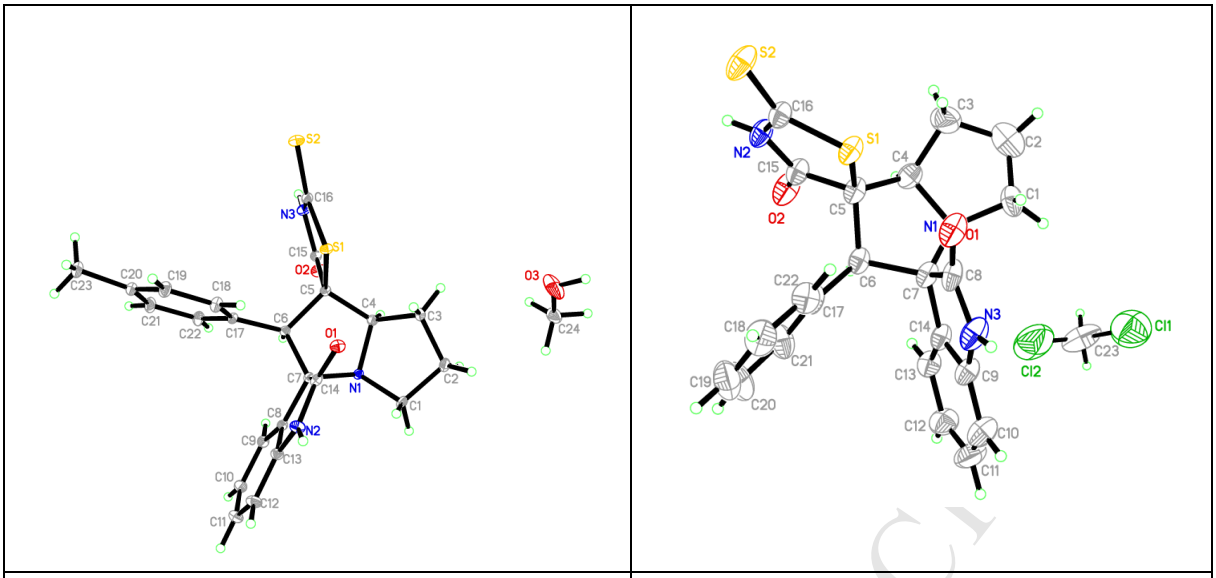

4a	4b

Figure 1. ORTEP diagram of the compounds **4a** and **4b**. Displacement ellipsoids are plotted at 30% probability level.

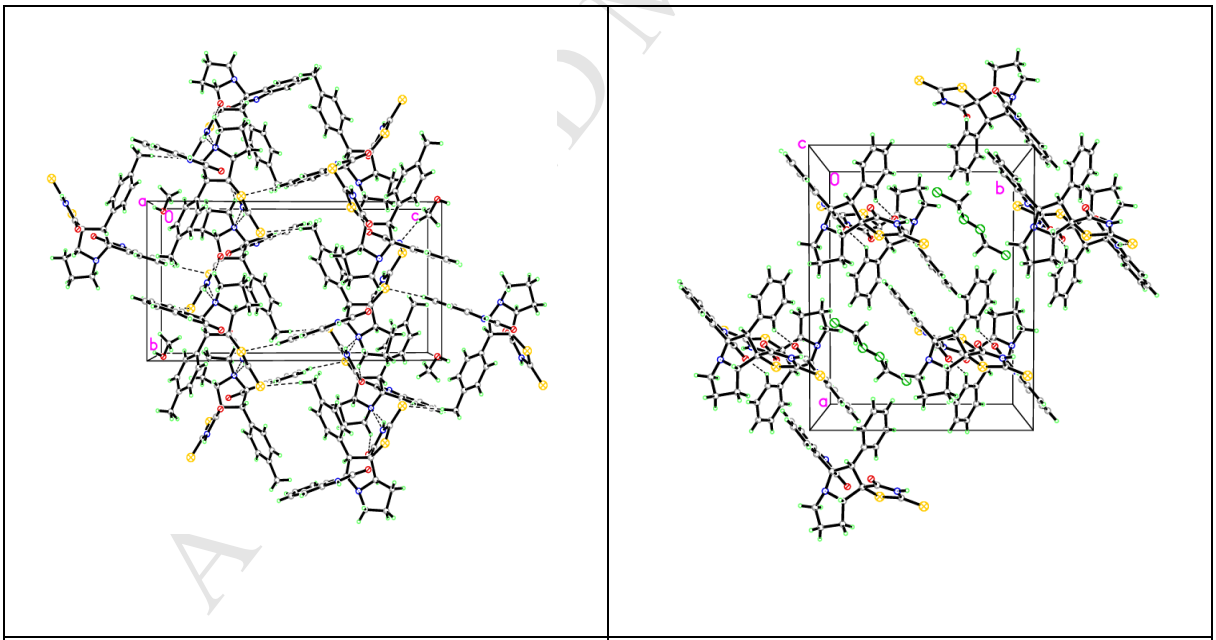

4a	4b

Figure 2. Crystal packing showing intermolecular hydrogen bonds as dashed lines.

Table 1. Crystal data and structure refinement for compounds **4a,b**.

Crystal data	**4a**	**4b**
Empirical Formula	$2(C_{23}H_{21}N_3O_2S_2)\cdot CH_4O$	$2(C_{22}H_{18}N_3O_2S_2)\cdot CH_2Cl_2$
Formula Weight	903.18	928.01
Temperature (K)	100(2)	(2) 293
Wavelength (Å)	Mo Kα radiation, 0.71073	Cu Kα radiation, 1.54178
Crystal system	Monoclinic	Monoclinic
Space group	*C*2/*c*	*C*2/*c*
Unit cell dimensions	*a* = 9.7855 (5) Å, α = 90.00° *b* = 10.4786 (5) Å, β = 92.662 (2)° *c* = 20.6713 (9) Å, γ = 90.00°	*a* = 17.0062 (10) Å, α = 90.00° *b* = 13.3291 (9)Å, β = 93.210 (4)° *c* = 20.3259 (14) Å, γ = 90.00°
Volume ($Å^3$)	2117.31 (17)	4600.2 (5)
Z, calculated density ($mg.m^{-3}$)	2, 1.417	4, 1.340
Absorption coefficient (mm^{-1})	0.28	3.36
F(000)	948	1928
Crystal size (mm)	0.40 × 0.29 × 0.14	0.62 × 0.48 × 0.39
Theta range for data collection (^{o})	2.8° to 33.2°	4.2° to 69.4°

Limiting indices	-11 ≤h ≤11, -12 ≤k ≤12, -24 ≤l ≤24	-19 ≤h ≤19, -15 ≤k ≤14, -23 ≤l ≤22
Reflections collected /unique	50446 / 3658 [R(int) = 0.039]	24566 / 3372 [R(int) = 0.114]
Completeness to theta	25.0° (100 %)	69.4° (100 %)
Refinement method	Full-matrix least-squares on F^2	Full-matrix least-squares on F^2
Data/ restraints/ parameters	3735 / 0 /295	3665 / 0 /289
Goodness of- fit on F^2	1.08	1.08
Final R indices [I > 2σ(I)]	R1 = 0.039, wR2 = 0.053	R1 = 0.114, wR2 = 0.076
R indices (all data)	R1 = 0.0532, wR2 = 0.136	R1 = 0.0765, wR2 = 0.206
Largest diff. peak and hole (e A^{-3})	0.82 and −0.70	1.15 and -0.47
CCDC reference	1425092	1424967

Table 2 Selected geometric parameters (Å, °) of **4a**.

S1—C5	1.815 (3)	N1—C1	1.521 (4)
S1—C16	1.765 (3)	N1—C7	1.514 (4)
S2—C16	1.668 (3)	N2—C14	1.349 (4)
O1—C14	1.223 (4)	N2—C13	1.408 (4)
O2—C15	1.214 (4)	N3—C16	1.340 (4)

O3—C24	1.426 (8)	N3—C15	1.370 (4)
N1—C4	1.540 (4)		
C5—S1—C16	92.49 (14)	N1—C7—C14	108.8 (2)
C1—N1—C4	108.2 (2)	N1—C7—C6	100.0 (2)
C4—N1—C7	107.8 (2)	N2—C13—C8	109.8 (2)
C1—N1—C7	118.5 (2)	N2—C13—C12	127.8 (3)
C13—N2—C14	112.0 (2)	O1—C14—C7	125.4 (3)
C15—N3—C16	113.5 (2)	N2—C14—C7	107.8 (2)
N1—C1—C2	103.7 (2)	O1—C14—N2	126.8 (3)
N1—C4—C3	104.7 (2)	O2—C15—N3	124.7 (3)
N1—C4—C5	106.0 (2)	O2—C15—C5	120.0 (3)
S1—C5—C15	103.03 (19)	N3—C15—C5	115.3 (2)
S1—C5—C6	117.7 (2)	S2—C16—N3	126.3 (2)
S1—C5—C4	116.2 (2)	S1—C16—N3	114.8 (2)
N1—C7—C8	113.3 (2)	S1—C16—S2	118.93 (17)

Table 3. Hydrogen-bond geometry (Å, °) of **4a**.

D—H···A	D—H	H···A	D···A	D—H···A
N2—H1N2···S2^{i}	0.89(4)	2.45(4)	3.306(2)	161(3)
N3—H3D···N1^{ii}	0.8800	1.9800	2.745(3)	144.00
C1—H1A···O2^{iii}	0.9900	2.4500	3.087(4)	122.00

C2—H2A···O2^{iii}	0.9900	2.5800	3.250(4)	125.00
C3—H3A···O1	0.9900	2.5400	3.203(4)	124.00
C9—H9A···S2^{iii}	0.9500	2.7700	3.705(3)	170.00
C24—H24C···N2^{i}	0.9800	2.5000	3.447(6)	162.00

Symmetry codes: (i) −*x*+2, *y*+1/2, −*z*+3/2; (ii) −*x*+1, *y*−1/2, −*z*+3/2; (iii) −*x*+1, *y*+1/2, −*z*+3/2.

Table 4 Selected geometric parameters (Å, °) of **4b**.

C11—C23	1.820 (18)	N1—C4	1.506 (5)
C12—C23	1.564 (19)	N1—C1	1.492 (6)
S1—C16	1.730 (4)	N1—C7	1.482 (5)
S1—C5	1.830 (4)	N2—C8	1.359 (6)
S2—C16	1.645 (4)	N2—C9	1.408 (6)
O1—C8	1.214 (6)	N3—C16	1.348 (5)
O2—C15	1.208 (5)	N3—C15	1.367 (5)
C5—S1—C16	93.51 (18)	N1—C7—C14	116.2 (3)
C1—N1—C4	107.9 (3)	O1—C8—C7	125.9 (4)
C1—N1—C7	119.4 (3)	N2—C8—C7	107.6 (4)
C4—N1—C7	110.5 (3)	O1—C8—N2	126.5 (4)
C8—N2—C9	112.3 (3)	N2—C9—C10	128.6 (4)
C15—N3—C16	117.5 (3)	N2—C9—C14	108.8 (4)
N1—C1—C2	103.1 (4)	N3—C15—C5	112.8 (3)

N1—C4—C3	105.5 (4)	O2—C15—N3	124.0 (4)
N1—C4—C5	106.0 (3)	O2—C15—C5	123.1 (4)
S1—C5—C6	117.4 (2)	S1—C16—N3	112.0 (3)
S1—C5—C15	104.1 (3)	S2—C16—N3	124.9 (3)
S1—C5—C4	115.9 (3)	S1—C16—S2	123.1 (2)
N1—C7—C6	101.7 (3)	Cl1—C23—Cl2	113.1 (10)
N1—C7—C8	112.9 (3)		

Table 5. Hydrogen-bond geometry (Å, °) of **4b**.

D—H···A	D—H	H···A	D···A	D—H···A
N2—H2C···S2^{i}	0.8600	2.6600	3.512 (3)	173.00
N3—H3C···N1^{ii}	0.8600	2.0000	2.863 (4)	176.00
C1—H1A···O2^{iii}	0.9700	2.4600	3.313 (6)	147.00
C1—H1B···O1	0.9700	2.3800	3.087 (5)	129.00
C20—H20A···O2^{iv}	0.9300	2.5600	3.488 (6)	173.00
C22—H22A···O1^{i}	0.9300	2.4800	3.251 (5)	140.00
C23—H23A···O2^{v}	0.9700	2.4100	3.307 (17)	153.00

Symmetry codes: (i) −*x*−3/2, −*y*−3/2, −*z*+1; (ii) −*x*−3/2, *y*−1/2, −*z*+1/2; (iii) −*x*−3/2, *y*+1/2, −*z*+1/2; (iv) −*x*−1, *y*, −*z*+1/2; (v) −*x*−3/2, −*y*−1/2, −*z*.

3.3. Hirshfeld surface analysis

The Hirshfeld surfaces (HS) mapped over d_{norm} (A), shape index (B) and curvedness (C) for compound **4a** are shown in Figure 3. The overall fingerprint plots (FPs) and the decomposed ones for the most significant interactions are given in Figure S1 (Supplementary data). The decomposed FPs of the studied compounds shed the light on the effect of the H---H, H---C, S---H, O---H and N---H intermolecular interactions on the molecular structures of the studied compounds. The contributions of all possible intermolecular interactions in the crystal of both compounds are illustrated in Figure 4.

According to the crystallographic data obtained for the two compounds **4a** and **4b**, there are two main differences in their structures. The first difference is in the nature of the substituent at the phenyl ring and the second difference is the co-crystallization with methanol and dichloromethane solvent molecules in **4a** and **4b**, respectively. It is evident from Figure 3 that the main intermolecular interactions in both crystals are the same, except that **4b** also shows a significant amount of H---Cl interactions between the protons that are present inside the surface and the Cl atom of the solvent dichloromethane present in the crystal. These interactions appear as a sharp spike towards the left of the fingerprint plot (Figure S1, Supplementary data). The curvedness and shape index plots do not show any characteristic features of π-π stacking interactions, as evident from the absence of the blue and red triangles in the shape index as well as the absence of flat areas in the curvedness plot.

Front View	Back View	Front View	Back View
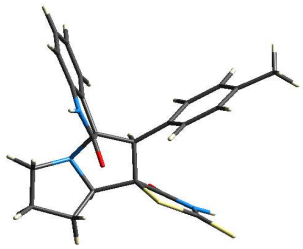	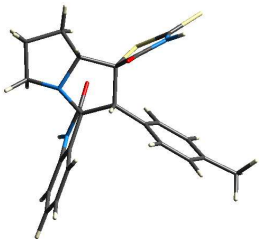	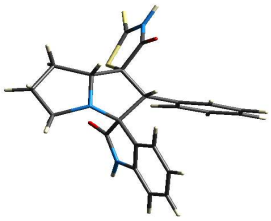	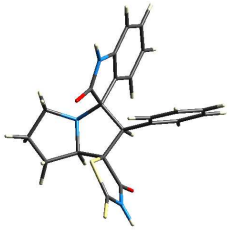
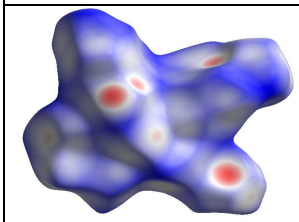	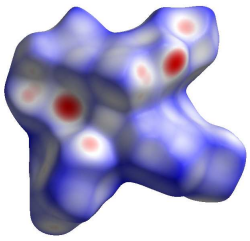	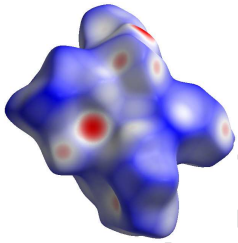	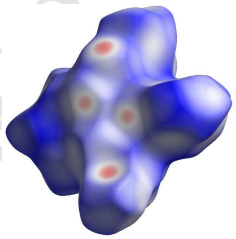
d_{norm}			
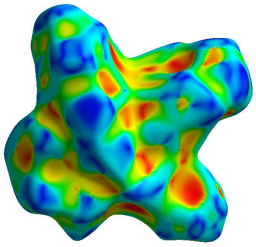	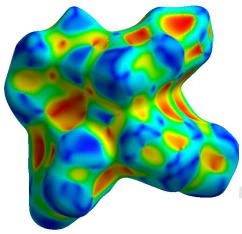	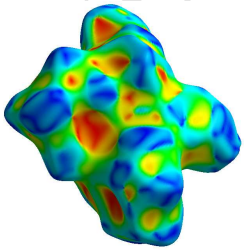	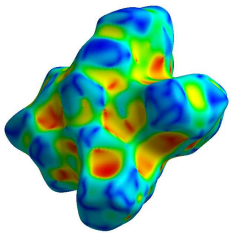
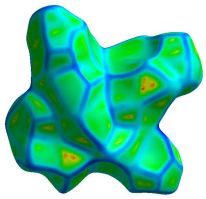	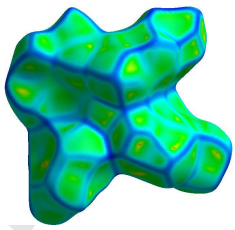	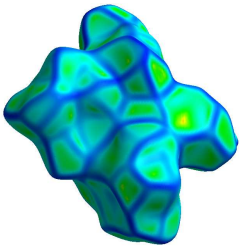	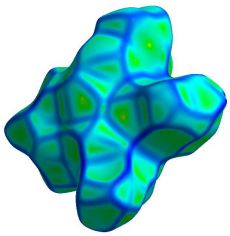
Curvedness			
4a		**4b**	

Figure 3. Hirshfeld surfaces of the molecules **4a** and **4b**.

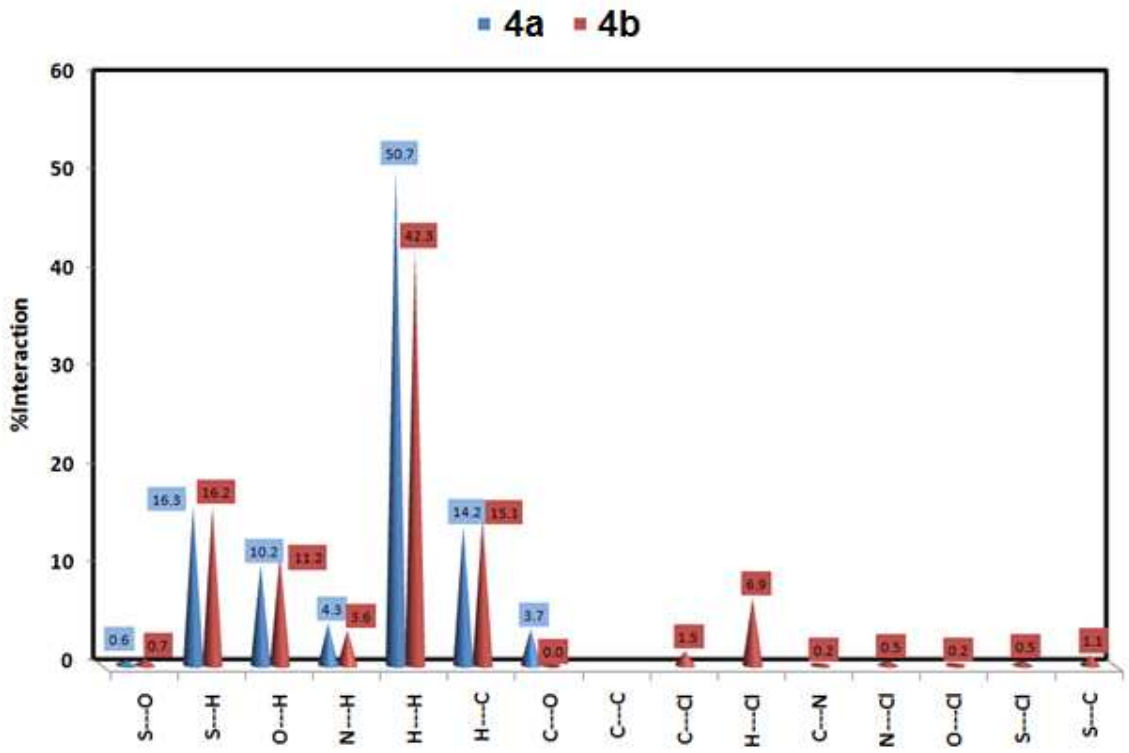

Figure 4. Percentage distribution of all possible interactions in the studied crystals.

3.4. DFT studies

The optimized structures of **4a** and **4b** were matched with their X-ray structures, and the results are shown in Figure 5. It is clear from these comparison graphs that there is a good agreement between the calculated and experimental structures. The results shown in Table S1 (Supplementary data) confirm this conclusion as well. The maximum deviation of the bond distances is not greater than 0.063 Å (4.2%) and 0.043 Å (2.9%) for **4a** and **4b**, respectively. In this regard, the energies of the highest occupied molecular orbital (HOMO) and the lowest unoccupied molecular orbital (LUMO) were computed using the same level of theory. These frontier molecular orbitals are important for understanding the electron transport processes in these compounds. These processes are important parameters for the biological applications of such molecular systems. A pictorial representation of these orbitals

is given in Figure 6. It is clear that changing the substituent has little effect on the HOMO and LUMO energies and geometries. The HOMO level is mainly localized over the thioxothiazolidin-4-one ring for both molecules while the LUMO level is mainly delocalized over the conjugated π-system in both compounds. The HOMO-LUMO energy gap of 4.053 eV is almost the same for both compounds.

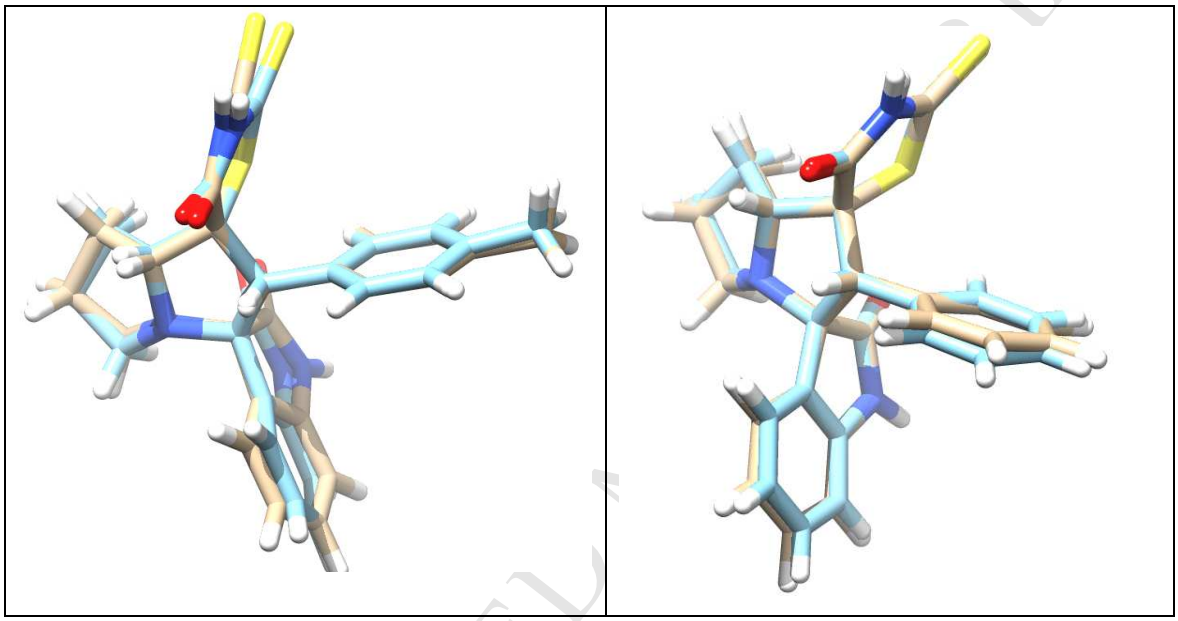

Figure 5. Structure matching of the calculated and experimental structures of the studied compounds **4a** and **4b**.

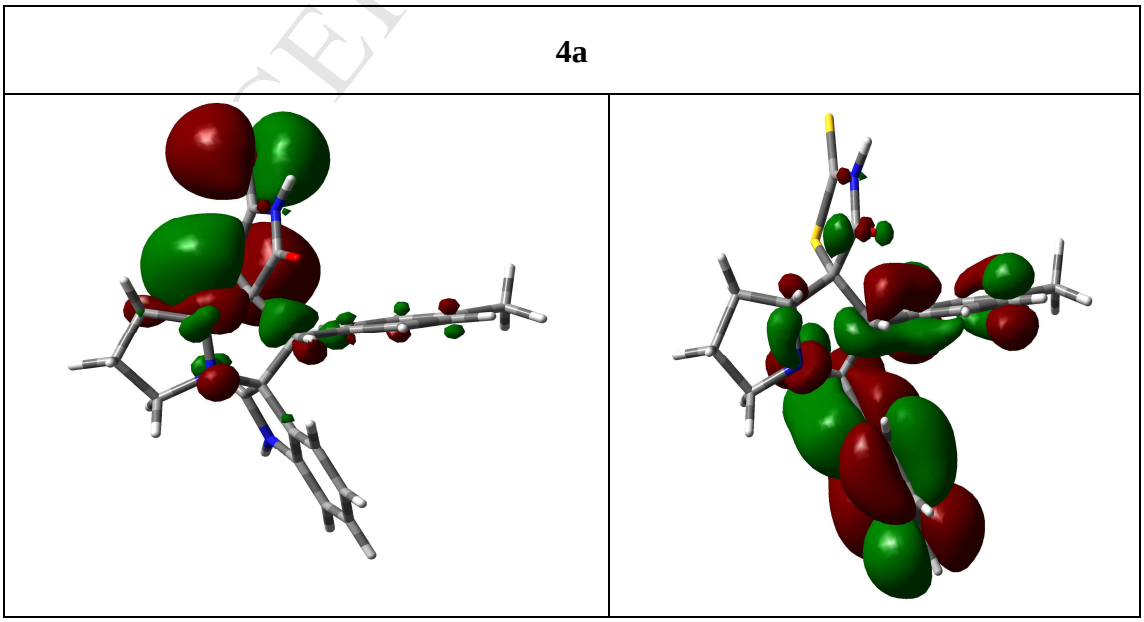

HOMO (-5.9743 eV)	LUMO (-1.9211 eV)
4b	
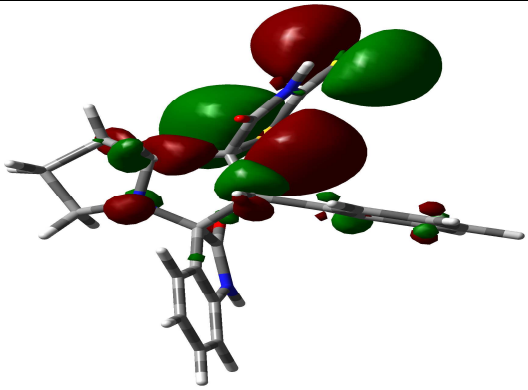	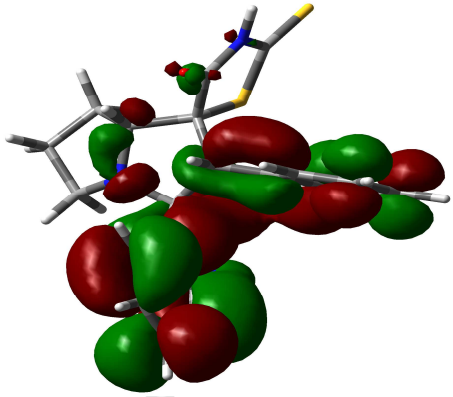
HOMO (-5.9991 eV)	**LUMO (-1.9464 eV)**

Figure 6. Frontier molecular orbitals of **4a** and **4b** calculated using B3LYP/6-311G(d,p) method.

3.5. Antimicrobial Evaluation

The synthesized spirooxindole derivatives **4a** and **4b** were tested for their antibacterial and antifungal activity at different concentrations in DMSO. Gentamicin and Ampicillin were used as the positive control drugs for antibacterial. Fluconazole and Amphoterecin-B were used as the positive control drugs for antifungal tests. The minimum concentration at which no growth was observed was taken as the minimum inhibitory concentration (MIC) value.

3.5.1. Antimicrobial Activity

Results of the biological activity were illustrated in Table 6; results are expressed as µg/mL inhibition. The antibacterial activity of synthesized compounds was elucidated against two gram positive strain and two gram negative strain namely *Streptococcus pneumonia, Bacillis subtilis, Pseudomonas aeruginosa, and Escherichia coli* respectively. Antibacterial activity of compounds 4a, and 4b were compared with the known ampicllin in case of gram positive bacteria and gentamicin in case of gram negative bacteria. Compounds **4a** and **4b** were more

active than standard drugs against all examined bacteria. Compound **4b** exhibited better activity than analogues **4a** in case of *S. pneumonia, B. subtilis,* and *E.coli* respectively. In case of activity against *P. aeruginosa*, compound **4b** showed MIC values of 15 while **4a** and gentamicin have MIC values of 16, 19 respectively.

Table 6. Antibacterial activity of compound **4a,b** showed in minimal inhibitory concentrations (MIC)

Compound	Gram Positive Bacteria		Gram Negative Bacteria	
	Streptococcus pneumoniae	***Bacillis subtilis***	***Pseudomonas aeruginosa***	***Escherichia coli***
	Ampicillin		**Gentamicin**	
Standard	25 ± 0.25	33 ± 0.32	19 ± 0.60	19.0 ± 0.33
4a	19 ± 0.40	28 ± 0.35	16 ± 0.15	18.5 ± 0.21
4b	23 ± 0.24	30 ± 0.55	15 ± 0.35	19.0 ± 0.33

Data are expressed as mean ± SD; Standard = 25 μg/mL.

3.5.2. Antifungal Activity

Based on antibacterial activity of our compounds, our attention was directed to extent the benefit of these interesting compounds to be broad spectrum antimicrobial especially in mixed infection disease. In this regard, compounds **4a** and **4b** were evaluated for their antifungal activity against *Aspergillus fumigates, Syncephalastrum racemosum, Geotricum candidum, and Candida albicans fungai*. The study was done by the diffusion method and serial dilution method [23].Their activities were compared with the known antifungal agents Fluconazole and Amphotericin B. Interestingly, both compounds **4a** and **4b** were more active than both standard against examined fungai. In a correlation manner, again compound **4b** was most active in this study. Theses correlation data and good activity guided us to understand the ode of interaction using molecular modeling study.

Table 7. Antifungal activity of the synthesized compound **4a,b** (Zone of inhibition; diameter in mm).

Compound	Fungal Strains			
	Aspergillus fumigates	***Syncephalastrum racemosum***	***Geotricum candidum***	***Candida albicans***
	Standard Drug			
I	23 ± 0.54	22.1 ± 0.20	29 ± 0.11	26 ± 0.22
II	25 ± 0.11	24.1 ± 0.15	30 ± 0.33	28 ± 0.55
4a	18 ± 0.46	19 ± 0.38	27 ± 0.18	27 ± 0.11
4b	16 ± 0.50	14 ± 0.47	24 ± 0.25	25 ± 0.19

Data are expressed as mean ± SD; standard = 25 μg/mL; I: Amphotericin B; II: Fluconazole.

3.6. Molecular docking

A library of target compounds and standard gentamicin and fluconazole drugs was designed and energy minimized using MMFF94 force field calculations. Aminoglycoside Phosphotransferase which was obtained from protein data bank (PDB code: 3HAM) [55] was selected as the target protein for antibacterial activity of our tested compound. Lanosterol 14 α-demethylase (CYP51A1) (PDB ID 4WMZ) [56] was chosen as a target protein for antifungal activity of our compounds

The docking study was prepared for docking using Open Eye® software. This software package generates consensus scoring which is a filtering processes to obtain virtual binding affinity, the lower consensus score, the better binding affinity of the ligands towards the receptor.

3.6.1. Molecular Docking as antibacterial

The study revealed that both compound **4b** and the standard drug gentamicin showed consensus score of 12 while compound **4a** showed consensus score 15. The standard gentamicin showed hydrogen bonds towards the binding site of ID: 3HAM with ASP:192:A, ASP:268:A, TYR:272:A (Fig. 7). However, compound **4a** showed a hydrophobic-hydrophobic interaction towards the binding site (Fig. 8). Furthermore, Compound **4b** showed a hydrogen bonding towards the binding site of ID: 3HAM coming from thiazolone NH (as donor) and carbonyl (as acceptor) functionalities with LYS:142:A and ASN: 191: A respectively (Fig. 9). Interestingly, compound **4b** (the most active derivative) occupied the receptor with pose and mode of interaction differs from the analogs **4a**. In case of **4b,** the carbonyl of thiazolone moiety is oriented close to phenyl arm (originated from benzaldehyde) while in **4a** the substituted phenyl arm (originated from *p*-methyl benzaldehyde) sets closely to carbonyl of indolone fragment**, (Fig. 10)**. This behavior suggests that the presence of *P* methyl group affect on the geometry of compound and so the strength and kind of interactions with target receptor.

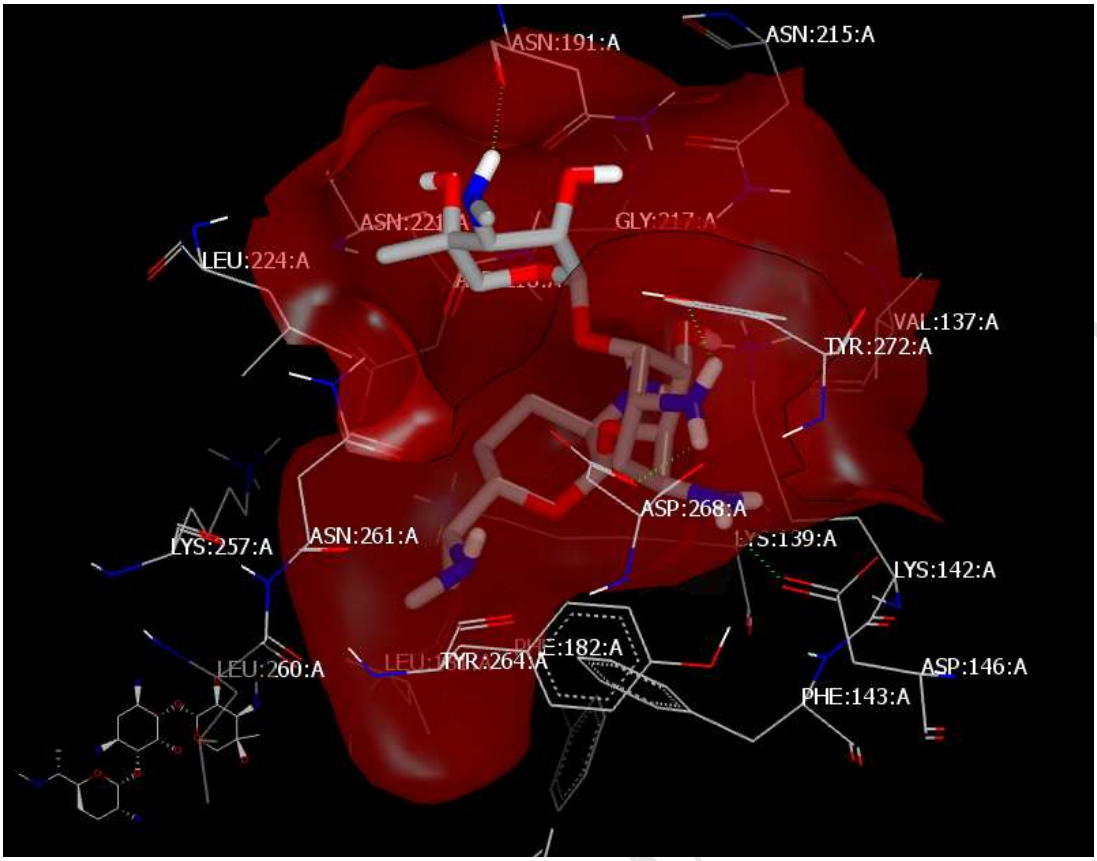

Figure 7: Visual representation for **gentamicin** docked with PDB: 3HAM showing the hydrophobic-hydrophobic interaction towards the binding site and the dashed green lines showing the hydrogen bonding

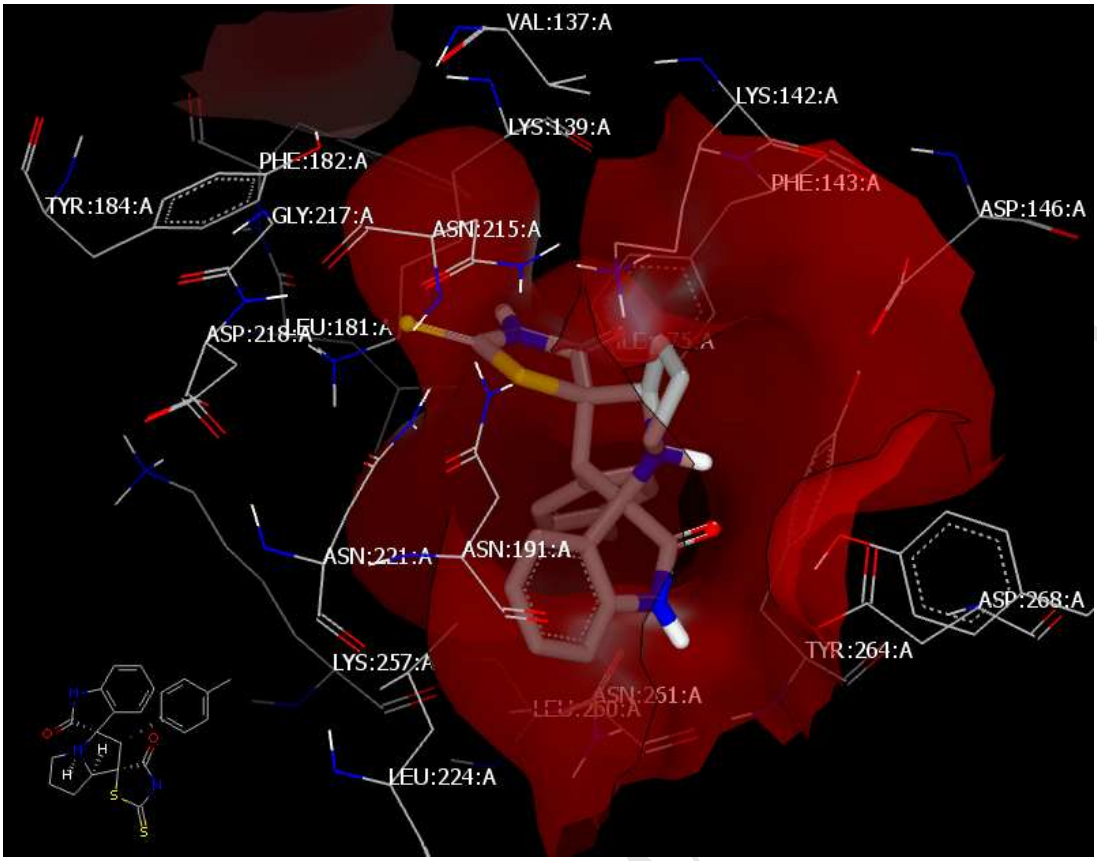

Figure 8: Visual representation for **4a** docked with PDB: 3HAM showing the hydrophobic-hydrophobic interaction towards the binding site and no detected hydrogen bonding

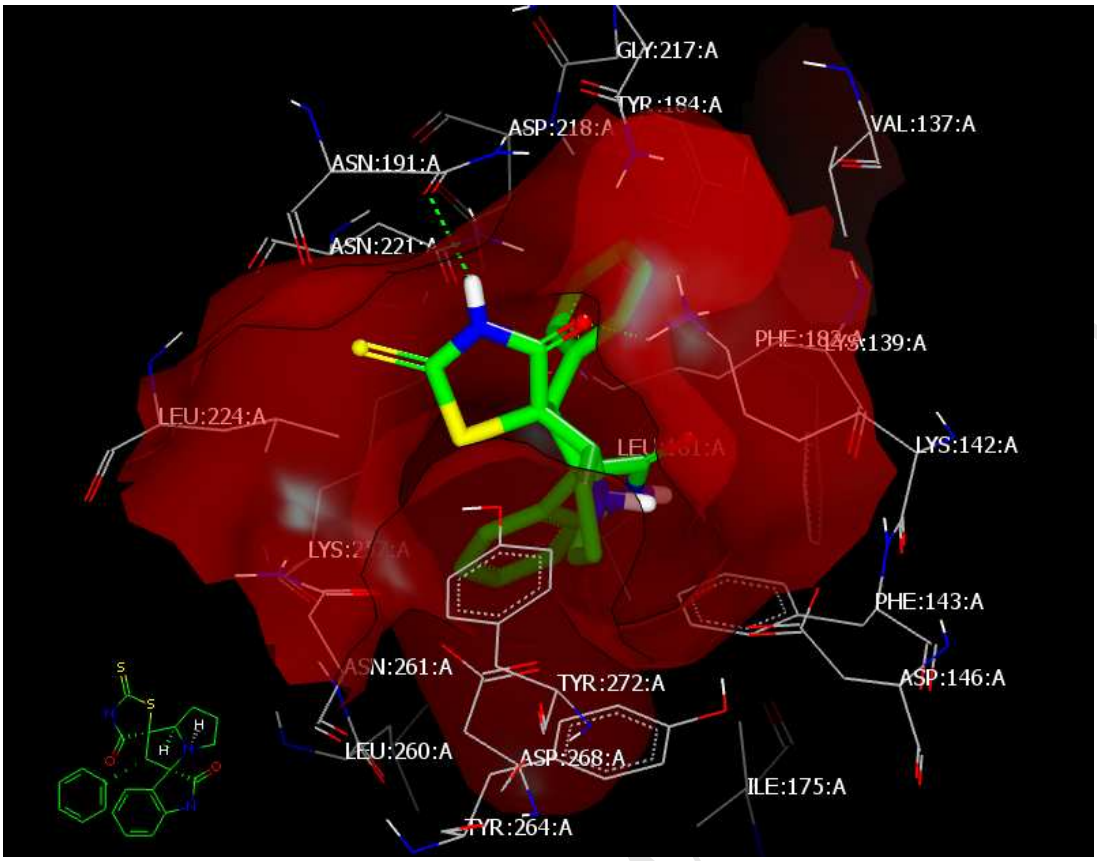

Figure 9: Visual representation for **4b** docked with PDB: 3HAM showing the hydrophobic-hydrophobic interaction towards the binding site and the dashed green lines showing the hydrogen bonding.

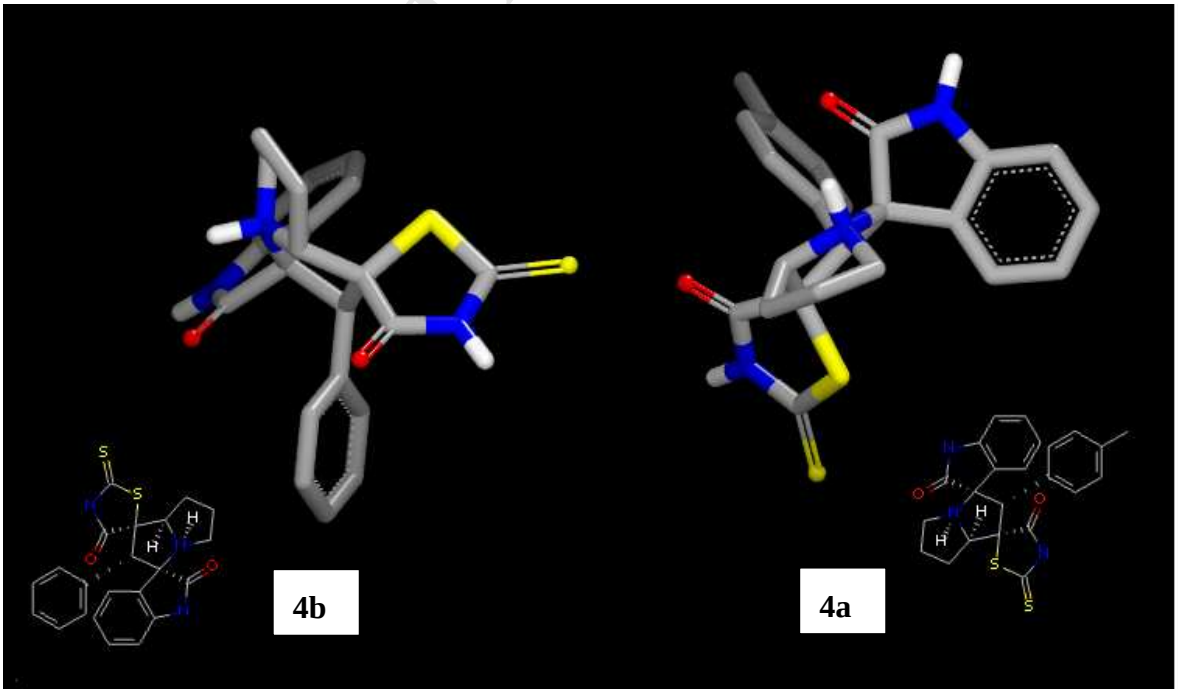

Figure 10: Visual representation for **4a and 4a conformers which docked** with PDB: 3HAM showing both compounds occupy the receptor with different geometry

3.6.2. Molecular Docking as Antifungal

The standard drug, fluconazole showed interaction with consensus score of 28 and interacts with the specific receptor through hydrophobic-hydrophobic and hydrogen bonding interactions. This docking mode similar to cocrystalized docking mode [50] (supplementary data) Compound **4a**, with a consensus score of 19, interacts with the receptor through its thiazolinone moiety and forms four hydrogen bondings with consequent amino acids in the receptor. It interacts with HIST: 468: A by thione functionality, ARG: 469 A and CYS: 470 A by NH part, and LEU: 471 A by oxygen of carbonyl, Fig. 11. However, compound **4b**, with a consensus score of 21, forms one hydrogen bonding with LEU: 471 A through oxygen of carbonyl in thiazolinone moiety, Fig. 12. Judging from docking study for compounds **4a**, and **4b** as antibacterial and antifungal, both compounds showed different pose and no exact similar mode of interaction. These results emphasize the importance of substituent of phenyl arm as important pharmacophore in this study.

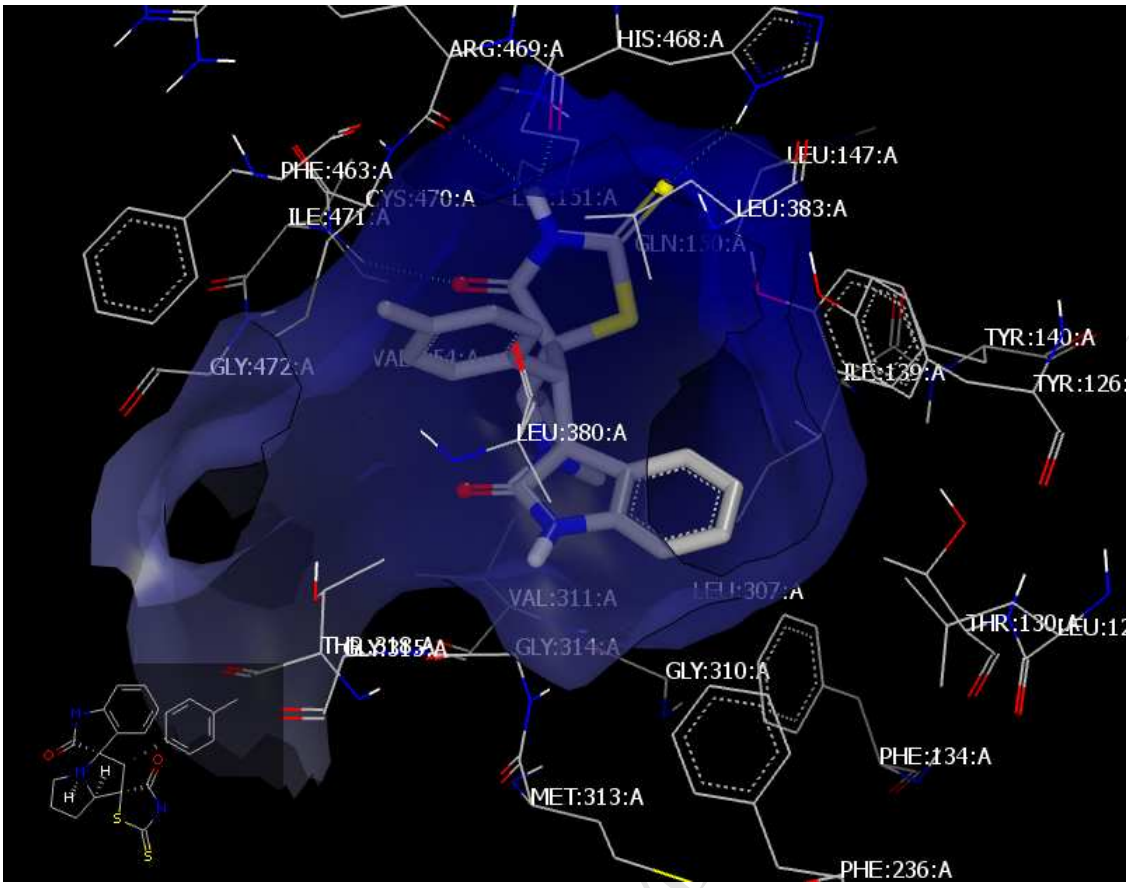

Figure 11: Visual representation for **4a** docked with PDB: 4WMZ showing the hydrophobic-hydrophobic interaction towards the binding site and the dashed green lines showing the four hydrogen bondings.

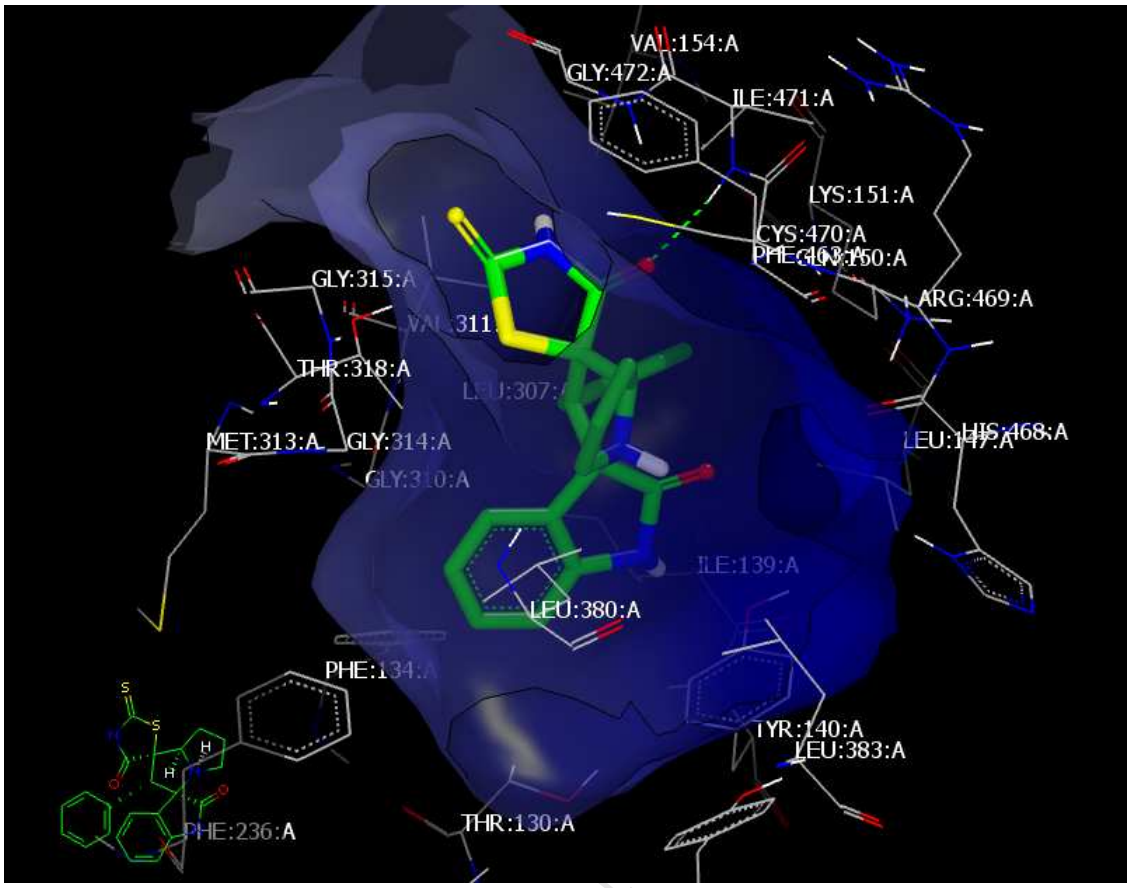

Figure 12: Visual representation for **4b** docked with PDB: 4WMZ showing the hydrophobic-hydrophobic interaction towards the binding site and one hydrogen bonding.

Conclusion

The 1,3-dipolar cycloaddition of azomethine ylide generated in situ from isatin and L-prolin to arylidinyl thioxothiazolidin-4-one afforded spiro-oxindole /pyrrolidine/ thioxothiazolidin-4-one derivatives in high yields. Compound **4b** docked with Aminoglycoside Phosphotransferase through hydrophobic-hydrophobic and the hydrogen bonding interactions. While compound **4a** docked with hydrophobic-hydrophobic interaction only. The synthesized compounds showed good activity against selected gram negative bacteria and examined fungai. Docking study revealed that presence of substituent on phenyl arm, which originated from aldehyde components, effect on the geometry of compound and

so control its mode and pose of interaction. This interesting behavior suggests these compounds as a suitable candidate for mixed infection cases especially in skin infections or wound infections. We are concern to continue study in such interesting hybrid compounds as a good candidate for antimicrobial activity.

Supplementary Materials: Figure S1 The full and decomposed fingerprint plots of the most significant intermolecular interactions in the studied compounds. **Figure S2.** ^{1}HNMR for the compound **4a. Figure S3.** ^{13}CNMR for the compound **4a.Table S1** The calculated and experimental geometric parameters (bond distances and angles) of the studied compounds.

Acknowledgments: The authors would like to extend their sincere appreciation to the Deanship of Scientific Research at King Saud University for providing funding to the research group. (No. RGP-257). Dr. Yaseen A. MM Elshaier acknowledges OpenEyse Company for supporting the academic license of OpenEye software which help in docking study.

Conflicts of Interest: The authors declare no conflict of interest.

References

[1]L.D. Quin, J. Tyrell, Fundamentals of Heterocyclic Chemistry: Importance in Nature and in the Synthesis of Pharmaceuticals; ISBN: 978-0-470-56669-5, Wiley: New York, U.S.A., (2010).

[2]A. Padwa, Synthetic Applications of 1,3-Dipolar Cycloaddition Chemistry Toward Heterocycles and Natural Products; John Wiley & Sons: (2002).

[3]R.A. Maurya, R. Nayak, C.N. Reddy, J.S. Kapure, J.B. Nanubolu, K.K. Singarapu, M. Ajitha, RSC Adv., 4(2014), 3230.

[4]C.V. Galliford, K.A. Scheidt, Angew. Chem. Int. Ed., 46 (2007), 8748.

[5]W.H. Wong, P.B. Lim, C.H. Chuah, Phytochemistry, 41 (1996), 313.

[6]C.B. Cui, H. Kakeya, H. Osada, Tetrahedron, 52 (1996), 12651.

[7]K. Ding, Y. Lu, N.Z. Coleska, S. Qiu, Y. Ding, W. Gao, J. Stuckey, K. Krajewski, P.P. Roller, Y. Tomita, D.A. Parrish, J.R. Deschamps, S. Wang, J. Am. Chem. Soc., 127 (2005), 10130.

[8]A. Padwa, W. Pearson, Synthetic Applications of Dipolar Cycloaddition Chemistry Towards Heterocyclic and Natural Product Chemistry; Eds.; Wiley VCH: Weinheim, Germany (2002).

[9]H. Dong, S. Song, J. Li, C. Xu, H. Zhang, L. Ouyang, Med. Chem. Lett., 25 (2015), 3585.

[10] F. von Nussbaum, Angew. Chem., Int. Ed. Engl., 42 (2003), 3068.

[11] S. Edmondson, S.J. Danishefsky, L. Sepp-Lorenzino, N. Rosen, J. Am. Chem. Soc., 121(1999), 2147.

[12] A. Fensome, W.R. Adams, A.L. Adams, T.J. Berrodin, J. Cohen, C. Huselton, A. Illenberger, J.C. Kern, V.A. Hudak, M.A. Marella, E.G. Melenski, C.C. McComas, C.A. Mugford, O.D. Slayden, M. Yudt, Z.M. Zhang, P.W. Zhang, Y. Zhu, R.C. Winneker, J.E. Wrobel, J. Med. Chem., 51 (2008), 1861.

[13] G. Wu, L. Ouyang, J. Liu, S. Zeng, W. Huang, B. Han, F. Wu, G. He, M. Xiang, Mol. Diversity, 17 (2013), 271.

[14] B. Yu, D.Q. Yu, H.M. Liu, Euro. J. Med. Chem., 97(2015)673.

[15] B. Yu, Z. Yu, P.P. Qi, D.Q. Yu, Euro. J. Med. Chem., 95 (2015)35.

[16] A Nefzi, J.M. Ostresh, R.A. Houghten, Chem. Rev., 97 (1997), 44.

[17] R.G. Frazen, J. Comb. Chem., 2(2000), 195.

[18] M.L. Barreca, E.D. Clercq, J. Med. Chem., 45 (2002), 5410.

[19] T. Zsolnai, Acad. Sci. Hung., 9 (1974), 125.

[20] C.R. Harris, S.A. Turnbull, Can. Entomol., 109 (1977), 1109.

[21] S.M. Prajapati, R.H. Vekariya, K.D. Patel, S.N. Panchal, H.D. Patel, D.P. Rajani, S. Rajani, Int. Lett. Chem. Phys. Astron., 20 (2014), 195.

[22] C. Shi, J. Zhou, Heterocycles 91(2015)1972.

[23] A. Barakat, H. J. Al-Najjar, A.M. Al-Majid, M.S. Soliman, Y.N. Mabkhot, M. H.M. Al-Agamy, H.A. Ghabbour, H-K. Fun, Journal of Molecular Structure 1081 (2015), 519.

[24] E.B. Akerblom, J. Med. Chem., 17 (1974), 609.

[25] S.S. Parmar, C. Dwivedi, A. Chaudhari, T.K. Guta, J. Med. Chem., 15 (1972), 99.

[26] R. Murugan, S. Anbazhagan, S.S. Narayanan, Euro. J. Med. Chem., 44(2009)3272.

[27] G.L. Feng, Y. Li, L.J. Geng, Journal of Chemical Research, 39(2015) 134.

[28] J. Li, J. Wang, Z. Xu, S. Zhu, ACS Comb. Sci., 16 (2014), 50.

[29] R.V.A. Orru, M. de Greef, Synthesis, 2003 (2003), 1471.

[30] M. Poornachandran, R. Raghunathan, Tetrahedron, 62 (2006), 11274.

[31] J. Yang, X.W. Liu, D.D. Wang, M.Y. Tian, S.N. Han, T.T. Feng, X.L. Liu, R.Q. Mei, Y. Zhou, Tetrahedron, 72 (2016), 8523.

[32] Y. Hu, Y. Zou, H. Wu, D. Shi, Ultrason. Sonochem., 19 (2012), 264.

[33] M. Hamzehloueian, Y. Sarrafi, Z. Aghaei, RSC Adv., 5 (2015), 76368.

[34] S. Ponnala, D.P. Sahu, R. Kumar, P.R. Maulik, J. Heterocycl. Chem., 43 (2006), 1635.

[35] H. Liu, Y. Zou, Y. Hu, D.Q. Shi, J. Heterocycl. Chem., 48 (2011), 877.

[36] G.S. Kumar, R. Satheeshkumar, W. Kaminsky, J. Platts, K.J.R. Prasad, Tetrahedron Lett., 55 (2014), 5475.

[37] M.J. Frisch, G.W. Trucks, H.B. Schlegel, G.E. Scuseria, M.A. Robb, J.R. Cheeseman. Gaussian–03, revision C.01. Wallingford, CT: Gaussian, Inc.; (2004).

[38] GaussView, Version 4.1, R. Dennington II, T. Keith, J. Millam, Semichem Inc., Shawnee Mission, KS (2007).

[39] S. K. Wolff, D.J. Grimwood, J. J. McKinnon, M. J. Turner, D. Jayatilaka, M. A. Spackman, Crystal Explorer 3.1 (2013), University of Western Australia, Crawley, Western Australia, 2005–2013, http://hirshfeldsurface.net/CrystalExplorer.

[40] F.L. Hirshfeld, Theor. Chem. Acc., 44 (1977), 129.

[41] M.A. Spackman, D. Jayatilaka, Cryst. Eng. Comm., 11 (2009), 19.

[42] J. Bernstein, R.E. Davis, L. Shimoni, N.L. Chang, Angew. Chem. Int. Ed. Engl., 34 (1995), 1555.

[43] S.K. Seth, I. Saha, C. Estarellas, A. Frontera, T. Kar, S. Mukhopadhyay, Cryst. Growth Des., 11 (2011), 3250.

[44] J.J. McKinnon, A.S. Mitchell, M.A. Spackman, Chem. Eur. J., 4 (1998), 2136.

[45] A. Parkin, G. Barr, W. Dong, C.J. Gilmore, D. Jayatilaka, J.J. McKinnon, M.A. Spackman, C.C. Wilson, Cryst. Eng. Comm., 9 (2007), 648.

[46] F.P. Fabbiani, L.T. Byrne, J.J. McKinnon, M.A. Spackman, Cryst. Eng. Comm., 9 (2007), 728.

[47] A.L. Rohl, M. Moret, W. Kaminsky, K. Claborn, J.J. McKinnon, B. Kahr, Cryst. Growth Des., 8 (2008), 4517.

[48] A. Barakat, H.A. Ghabbour, A.M. Al-Majid, S.M. Soliman, M. Ali, Y.N. Mabkhot, M.R. Shaik, H.-K. Fun, Molecules 20(2015) 13240.

[49] Fast Rigid Exhaustive Docking (FRED) Receptor, version 2.2.5; OpenEye Scientific Software, Santa Fe, NM (USA); http://www.eyesopen.com.

[50] OMEGA, version 2.5.1.4; OpenEye Scientific Software, Santa Fe, NM (USA); http://www.eyesopen.com.

[51] VIDA, version 4.1.2; OpenEye Scientific Software, Santa Fe, NM (USA); http://www.eyesopen.com.

[52] G. Lotfy, M.M. Said, H. El Sayed, H. El Sayed, A. Al-Dhfyan, Y.M.A. Aziz, A. Barakat, Bioorg. Med. Chem., 25 (2017), 1514.

[53] G.M. Sheldrick, Acta Crystallographica Section A: Foundations of Crystallography, A64 (2008), 112.

[54] Brucker. APEX2, SAINT and SADABS. Brucker AXS Inc., Madison, Wisconsin, U.S.A., (2009).

[55] P.G. Young, R. Walanj, V. Lakshmi, L.J. Byrnes, P. Metcalf, E.N. Baker, S.B. Vakulenko, C.A. Smith, J. Bacteriol., 191 (2009), 4133.

[56] A.A. Sagatova, M.V. Keniya, R.K. Wilson, B.C. Monk, J.D. Tyndall, Antimicrob.Agents Chemother. 59 (2015) 4982.

Highlights

- New regioselective spiro heterocycles **4a,b** were synthesized.
- The crystal structure of **4a,b** were reported.
- Hirshfeld surface analysis were reported.
- The HOMO–LUMO energies and related molecular properties were evaluated.
- Anti-microbial activity of the synthesized compounds are discussed.
- Molecular docking study of the synthesized compounds are presented.